Korean J. Chem. Eng., **29**(1), 54-58 (2012)
DOI: 10.1007/s11814-011-0146-x

Preparation of nanostructured TiO_2 thin films by aerosol flame deposition process

Jinrui Ding and Kyo-Seon Kim†

Department of Chemical Engineering, Kangwon National Univerisy, Chuncheon, Kangwon 200-701, Korea
(*Received 1 April 2011 • accepted 3 June 2011*)

Abstract–Titania thin films were prepared by using aerosol flame deposition process via the pyrolysis of titanium tetra-isopropoxide (TTIP) precursor. We analyzed the specific surface area, primary and secondary particle sizes, crystal structure, thin film morphology and thickness by BET method, electrophoretic light scattering, X-ray diffraction and scanning electron microscopy, respectively. The specific surface area of TiO_2 particles deposited is over three-times larger than that of commercial Degussa P25. Crystallite structure of TiO_2 particles can be controlled by changing the ratio of CH_4/O_2 flow rates. We could prepare TiO_2 thin films with single anatase phase by keeping the ratio of CH_4/O_2 flow rates at 200 ml/min: 1,000 ml/min. As N_2 carrier gas flow rate to bubbler increases, the primary and secondary particle sizes increase, but decrease with increasing total N_2 gas flow rate through the central tube. The shorter the deposition height is, the smaller the deposition area is, but the thin film becomes thicker in the central region.

Key words: TiO_2 Thin Films, TiO_2 Crystal Structure, Particle Deposition, Primary and Secondary Particle Sizes, AFD Process

INTRODUCTION

The aerosol flame deposition (AFD) process is used to prepare nano-sized metal oxide films from liquid precursors. The advantages of this method are the rapid formation of nano-sized metal oxide particles, simple and low-cost production operating under ambient atmosphere, wide application of precursors and high deposition rate [1]. Numerous studies have been carried out to synthesize metal oxide thin films for various applications by using AFD process [1-3]. TiO_2 nanoparticles have been produced by using diffusion flame reactor based on liquid precursor (titanium tetraisopropoxide) decomposition reaction [4,5].

Titanium dioxide has a wide band-gap of 3.2 ev, which can be activated under ultraviolet light. It exists in three polymorphic phases: anatase, rutile and brookite. Among them, the anatase phase has the highest photocatalytic activity compared with the rutile and brookite phases [6]. However, the rutile structure is the most stable form at high temperature, and anatase and brookite both can be converted to rutile upon heating [7]. TiO_2 thin films have been widely used as photocatalysts, such as for photodegradation to remove volatile organic compounds [6] and also for photosplitting water to provide an environmentally benign and sustainable source of hydrogen fuel for the energy industry [8-10]. Another prominent role which TiO_2 has played in the solar energy technology is in dye-sensitized solar cells. TiO_2 is the electron conduction layer in the dye-sensitized solar cells which are inexpensive and economically viable alternatives to conventional silicon-based technology [11,12]. All these solar energy applications of TiO_2 require that TiO_2 film has large surface area either for high solar energy harvesting or for large interpenetrated interface. Nanoparticles are typically used to fabricate photocatalytic TiO_2 films owing to their high specific surface area [12,13]. It's critical to control the particle size as deposited and the morphology of thin films.

In our present work, we prepared TiO_2 thin films by AFD process and analyzed the effects of various process parameters such as the N_2 carrier gas flow rate to bubbler, total N_2 gas flow rate through the center tube and deposition height on the properties of TiO_2 thin films. The changes of primary and secondary particle sizes and the thickness distribution of TiO_2 thin films on substrate were examined.

EXPERIMENTAL SECTION

Fig. 1 shows the schematic of the experimental setup for TiO_2

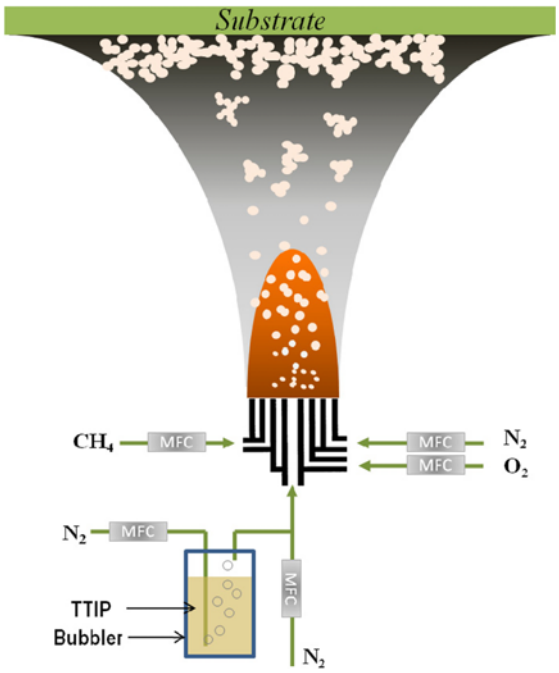

Fig. 1. Schematic diagram of an AFD apparatus.

†To whom correspondence should be addressed.
E-mail: kkyoseon@kangwon.ac.kr

thin film deposition. The substrate is kept above the burner by a holder. The precursor of TiO_2, titanium tetraisopropoxide (TTIP, $Ti(C_3H_7O)_4$), is contained in a bubbler, and the mass flow rate of TTIP is controlled by the N_2 carrier gas flow rate to the bubbler. TTIP vapor was carried through the central tube to the burner tip. To maintain the gas flow rate to the central tube constant, an auxiliary N_2 gas flow was introduced to the central tube. O_2 of 1 L/min and 200 ml/min methane as fuel were supplied to the second and the third concentric tubes, respectively. The ambient N_2 gas of 250 ml/min was provided through the fourth concentric tube. The combustion of CH_4 takes place just after the burner tip. TTIP decompose to form TiO_2 particles at high temperature in the oxy-CH_4 flame. By thermophoresis and diffusion, TiO_2 particles finally deposit on the silicon wafer substrate to form thin film. In our study, first, TiO_2 thin films were prepared by maintaining total flow rate of N_2 through the central tube at 400 ml/min while varying the carrier gas flow rate to bubbler from 100 to 300 ml/min, which means the gas residence time was kept constant. Second, we changed the total carrier gas flow rate of N_2 through the central tube from 300 to 500 ml/min while keeping the carrier gas flow rate constant at 200 ml/min, which means the mass flow rate of TTIP was kept constant. We also investigated the effect of the distance between substrate and burner (10 cm and 7 cm) on the thickness distribution of deposited thin film and the crystal phase. The bubbler and precursor delivery tubes were heated to 80 °C to prevent TTIP condensation.

The TiO_2 thin films were deposited on silicon wafer. By scraping the wafer with a blade, TiO_2 particles were collected. The specific surface area (SSA, m^2/g) was measured by using the Brunauer-Emmett-Teller (BET) method (ASAP 2020, Micromeritics). The TiO_2 samples were degassed at 200 °C for 10 hours to remove gases and moisture from the surface by flowing N_2 for BET measurement. Assuming all particles to be monodisperse spherical particles, the BET-equivalent particle diameter, d_{BET} (nm), was calculated as follows [14]:

$$d_{BET} = \frac{6}{(\rho_P \times SSA)} \quad (1)$$

where ρ_p is the particles density (g/m^3), and we considered ρ_p as 4.0 g/m^3. The secondary particle size of TiO_2 was characterized by electrophoretic light scattering (ELS). Before analysis by ELS, samples were dispersed in deionized water with sonication for 1 hour at room temperature. The ELS analysis was performed with ELS-8000 (photal Otsuka Electronisc). The crystal phase was determined by X-ray diffraction (XRD). The XRD measurements were operated by using PW3040/60 X'Pert PRO (PANalytical) instrument using Ni filtered Cu Kα radiation (wavelength=1.54 Å). 2θ scan ranges from 20° to 80° and scanning step size of 0.02° were used. To measure the thickness of thin films, we fixed the glass slide to the wafer by binder clip before deposition. TiO_2 thin films were deposited on the glass slide and also on the wafer. Then, the glass slide with TiO_2 thin film was cut to several pieces at even intervals to measure the distribution of film thickness in cross-section by scanning electron microscopy (SEM, S-4300, Hitachi).

RESULTS AND DISCUSSION

Methane combustion reaction took place at the burner tip and provided energy for TTIP decomposition. When the N_2 gas carried TTIP vapor to the burner tip, it was immediately decomposed to form tiny TiO_2 monomer particle in the oxy-CH_4 flame. The decomposition reaction of TTIP is shown as follows:

$$TTIP \rightarrow TiO_2 + 4C_3H_6 + 2H_2O \quad (2)$$

with a reaction rate constant $k=3.96\times105\exp(-8479.7/T)$ for T=500-670 K [15]. Once the TTIP decomposition reaction occurs, TiO_2 monomers are generated. They collide with each other and coalesce to form single larger spherical particles upon passing the high flame temperature region where the coalescence rate might be faster than the collision rate. Later on, in the downstream region, where the flame temperature cools down, the coalescence rate becomes slower than the collision rate of particles, so the particles are covalently bonded with each other by sintering necks and become the aggregates. Further downstream, the aggregates collide with other particles to form the agglomerates which can be easily broken down into the aggregates because the temperature there is too low for sintering, and they hold each other by van der Waals forces rather than chemical interactions. The deagglomeration process can be accomplished by dispersing them in proper solutions and appropriate external forces such as mechanical stirring or sonication [16].

It is well known that photocatalytic activity of TiO_2 is also influenced by crystal structure, which is strongly affected by flame temperature. We prepared TiO_2 thin films for different ratios of CH_4/O_2 flow rates. As CH_4 flow rate decreases from 300 to 200 ml/min, it can be seen from Figs. 2(a) and (b) that the flame height becomes shorter, and the flame temperature correspondingly decreases. XRD patterns in Fig. 2(c) show that, for CH_4 flow rate of 200 ml/min, the prepared TiO_2 films have the single crystal anatase phase. However, for the case of 300 ml/min, the flame temperature increases and the rutile phase appears. Thus, we can see that by changing the

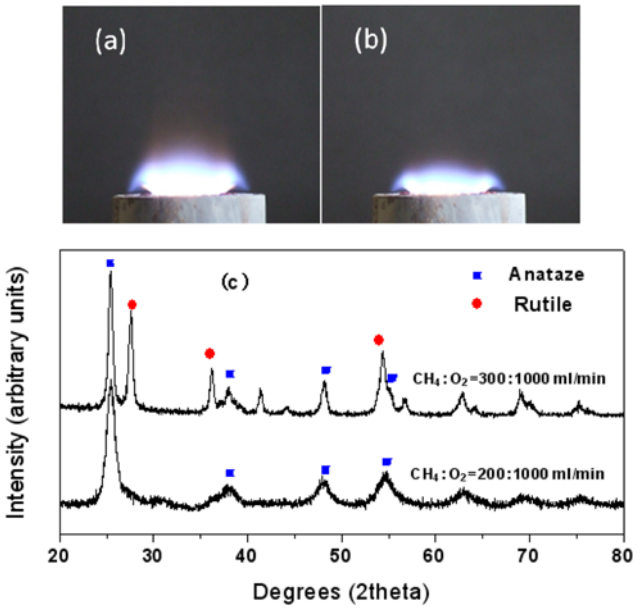

Fig. 2. Photographs of oxy-methane flame at (a) $CH_4 : O_2$=300 : 1,000 ml/min, (b) $CH_4 : O_2$=200 : 1,000 ml/min; (c) X-ray diffraction patterns of TiO_2 nanoparticles collected from silicon wafer substrates for various CH_4 flow rates.

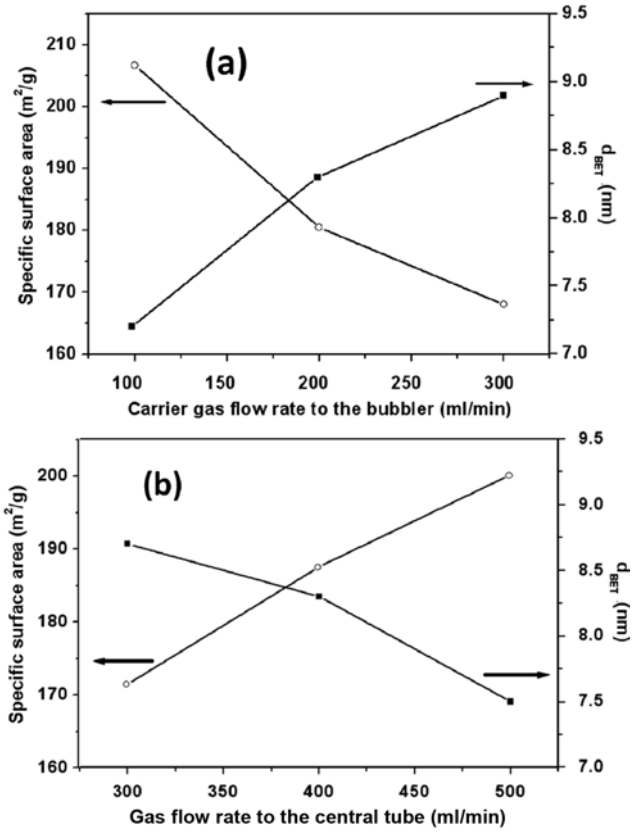

Fig. 3. Specific surface area and BET equivalent diameters (d_{BET}) of particles collected from silicon wafer substrates (a) for different N_2 carrier gas flow rate to the bubbler, (b) for different N_2 gas flow rate to the central tube (CH_4 : O_2=200 : 1,000 ml/min, deposition time=30 min, deposition height= 10 cm above the burner).

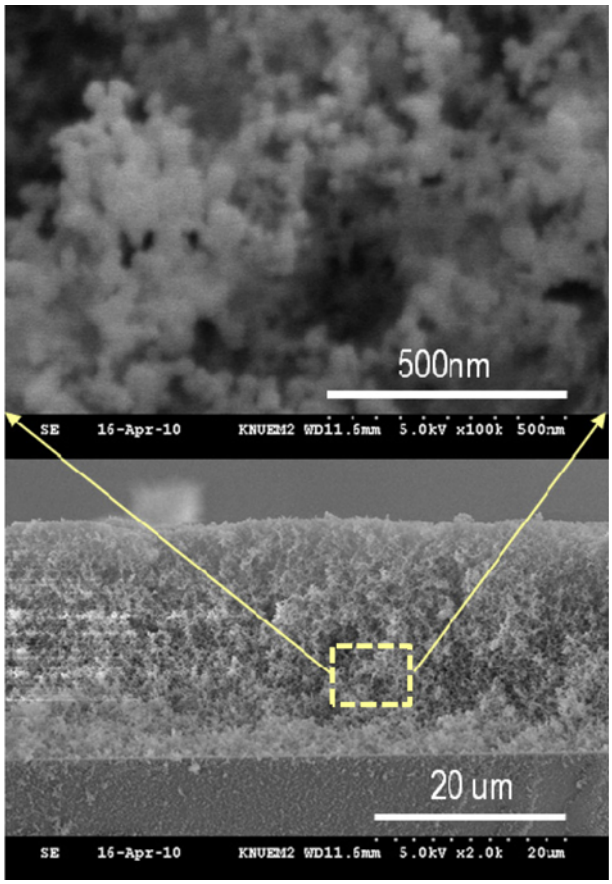

Fig. 4. Cross-sectional SEM images of TiO_2 thin film (CH_4 : O_2= 200 : 1,000 ml/min, carrier gas N_2 flow rate to the bubbler: 200 ml/min, N_2 gas flow rate to the central tube: 400 ml/min, deposition time=30 min, deposition height=10 cm above the burner).

ratio of CH_4/O_2 flow rates we can control the amounts of anatase and rutile crystal structures.

By BET method, the specific surface area of TiO_2 particles was measured. We calculated the diameters of particles based on Eq. (1). In Fig. 3(a), as the N_2 carrier gas flow rate to bubbler increases, the specific surface area of particles decreases, which means that the primary particle size increases. By increasing N_2 carrier gas flow rate to bubbler, initial TTIP concentration becomes higher and more TiO_2 monomers are formed in the high temperature zone of flame. The increased number of monomers resulted in shorter collision time between particles [17] and also in larger particle size due to faster coagulation and sintering. However, as total N_2 gas flow rate to the central tube increases, the specific surface area increases, and the primary particle size decreases correspondingly as shown in Fig. 3(b). By increasing total gas flow rate to the central tube, the residence time of particles for coagulation at high temperature decreases and the resultant particle size decreases.

The surface area is also an important characteristic of photocatalytic TiO_2 particles. The specific surface area of the commercial TiO_2 Degussa P25 is 50.0 m^2/g [5]. The TiO_2 particles we prepared have the specific surface area larger than that of Degussa P25 by more than three times. Fig. 4 shows the cross-sectional SEM images of TiO_2 thin films. The morphologies of thin films are all similar in our experimental conditions. From this result, we can see that TiO_2 thin film has high porosity, which also leads to high surface area for photocatalysts.

To measure the secondary particle size (average aggregate size), the samples were dispersed in the deionized water with sonication for 1 hour at room temperature. By sonication, the agglomerated particles can be broken down into the aggregates which cannot be broken down into individual primary particle easily because of the strong covalent bond between primary particles. Right after sonication, the secondary particle sizes were analyzed by ELS. Fig. 5(a) and (b) show the change of secondary particle size for various N_2 carrier gas flow rates to bubbler and also for various total gas flow rates of N_2 through the central tube, respectively. We can see that the secondary particle size increases with increasing N_2 carrier gas flow rate to bubbler, but decreases with increasing total gas flow rate of N_2 through the central tube. A higher N_2 carrier gas flow rate to bubbler leads to a higher initial TTIP concentration; thus, more particles generated in the high temperature region. Therefore, the bigger aggregates are formed by faster coagulation and sintering. By increasing total gas flow rate of N_2 to the central tube, the residence time of aggregates in the high temperature flame region decreases, and the secondary particle size decreases correspondingly.

We prepared TiO_2 thin films with different deposition height (7 cm

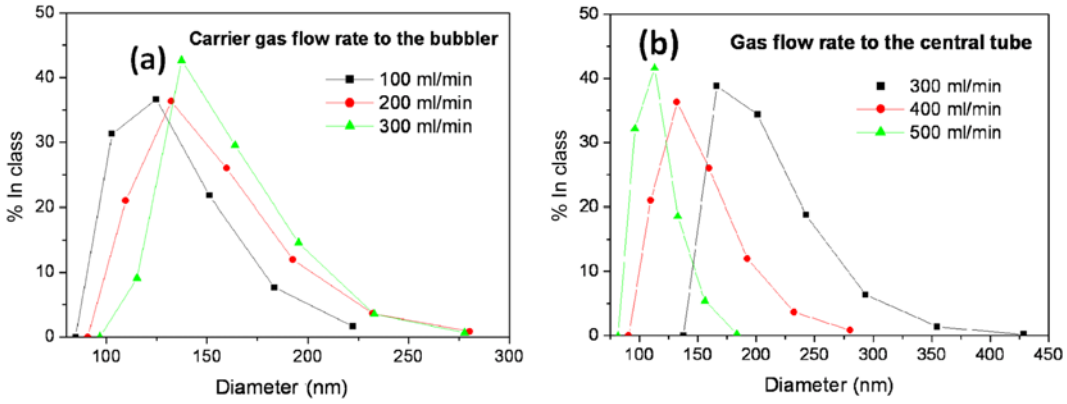

Fig. 5. Secondary particle size distributions by ELS based on number of TiO_2 particles prepared by changing (a) carrier gas N_2 flow rate to the bubbler from 100 to 300 ml/min, (b) total N_2 gas flow rate through the central tube from 300 to 500 ml/min (CH_4 : O_2=200 : 1,000 ml/min, deposition time=30 min, deposition height=10 cm above the burner).

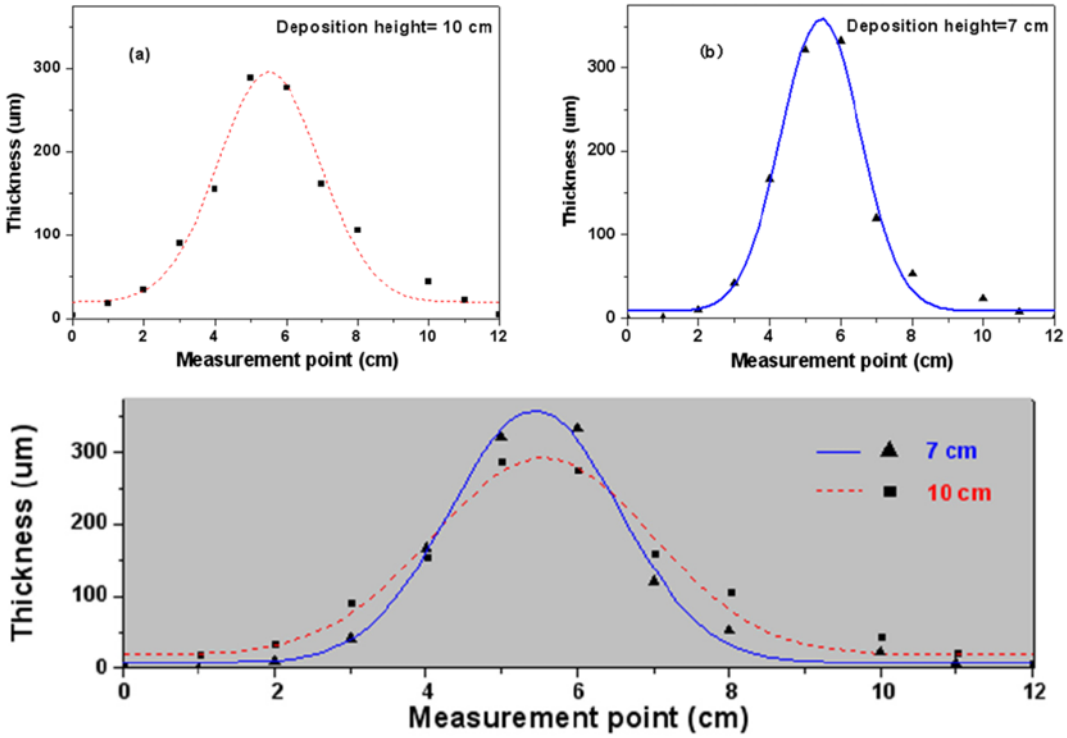

Fig. 6. The distribution of film thickness deposited on substrate for deposition height of (a) 10 cm, (b) 7 cm above the burner (carrier gas N_2 flow rate to the bubbler: 200 ml/min, CH_4 : O_2=200 : 1,000 ml/min, deposition time =30 min, N_2 gas flow rate to the central tube: 400 ml/min).

and 10 cm) to examine the distribution of film thickness on substrate. The thickness was measured through the cross-sectional SEM image. From Fig. 6, we can see that the shorter the distance between substrate and burner is, the smaller deposition area on substrate is, but the thicker the film thickness is in the central region of flame. The generated particles are transported by the convective flow and thermophoretic force as well as diffusion of particles. As the deposition height increases, more particles are diffused in the radial direction, which leads to the larger deposition area. The shorter distance between substrate and burner results in steeper gas temperature gradient and the thermophoretic deposition rate of TiO_2 particles onto the substrate increases, so the thickness of thin film in the central region prepared with 7 cm deposition height is thicker than that prepared with 10 cm deposition height.

CONCLUSIONS

Nanostructured TiO_2 thin films were prepared by AFD process for various process conditions of different gases flow rate, TTIP vapor concentration and deposition height. The prepared TiO_2 particles have a specific surface area three-times larger than that of commercial Degussa P25. Crystallite structure of TiO_2 particles could be controlled by changing the ratio of CH_4/O_2 flow rates. We prepared TiO_2 thin films with single anatase phase by keeping the CH_4 and

O_2 flow rates of 200 and 1,000 ml/min, respectively. As N_2 carrier gas flow rate to bubbler increases, the primary and secondary particle sizes increase. However, the primary and secondary particle sizes decrease with increasing total gas flow rate of N_2 through the central tube. We also examined the dependence of thin film thickness and deposition area on the distance between substrate and burner tip. The shorter the deposition height is, the smaller deposition area is, but the thin film is thicker in the central region. This study provides necessary information for our further studies to make uniform coating on large surface area substrate using AFD process.

ACKNOWLEDGEMENTS

This research was performed for the Hydrogen Energy R&D Center, one of the 21st Century Frontier R&D Programs funded by the Ministry of Science and Technology of Korea. Instrumental analysis was supported from the central laboratory of Kangwon National University. ELS data were taken at the Korea Basic Science Institute, Chuncheon, Korea. This paper is dedicated to Prof. Son-Ki Ihm in honor of his retirement.

REFERENCES

1. T. Lee, K. Cho, J. Oh and D. Shin, *J. Power Sources*, **174**(2), 394 (2007).
2. G. Lim, H. Jeong, I. Hwang, B. Kim, K. H. Kim, J. Park and D. L. Cho, *Surface Coat. Technol.*, **204**(21-22), 3393 (2010).
3. Y. Yoon, J. Im, H. You and D. Shin, *J. Eur. Ceramic Society*, **27**(13-15), 4257 (2007).
4. P. Sunsap, D. J. Kim and K. S. Kim, *Ind. Eng. Chem. Res.*, **47**(7), 2308 (2008).
5. K. K. Akurati, A. Vital, G. Fortunato, R. Hany, F. Nueesch and T. Graule, *Solid State Sci.*, **9**(3-4), 247 (2007).
6. L. Znaidi, R. Séraphimova, J. F. Bocquet and C. Pommier, *Mater. Res. Bull.*, **36**(5-6), 811 (2001).
7. X. Chen and S. S. Mao, *Chem. Rev.*, **107**(7), 2891 (2007).
8. S. Nakabayashi, A. Fujishima and K. Honda, *Chem. Phys. Lett.*, **102**(5), 464 (1983).
9. E. Thimsen, N. Rastgar and P. Biswas, *J. Phys. Chem. C*, **112**(11), 4134 (2008).
10. J. Nowotny, C. C. Sorrell, T. Bak and L. R. Sheppard, *Sol. Energy*, **78**(5), 593 (2005).
11. J. W. Lee, K. J. Hwang, W. G. Shim, K. H. Park, H. B. Gu and K. H. Kwun, *Korean J. Chem. Eng.*, **24**(5), 847 (2007).
12. M. Grätzel, *J. Photochem. Photobiol. C: Photochem. Rev.*, **4**(2), 145 (2003).
13. M. K. Nazeeruddin, S. M. Zakeeruddin, J. Lagref, P. Liska, P. Comte, C. Barolo, G. Viscardi, K. Schenk and M. Graetzel, *Coord. Chem. Rev.*, **248**(13-14), 1317 (2004).
14. K. Wegner and S. E. Pratsinis, *AIChE J.*, **49**(7), 1667 (2003).
15. K. Nakaso, K. Okuyama, M. Shimada and S. E. Pratsinis, *Chem. Eng. Sci.*, **58**(15), 3327 (2003).
16. K. K. Akurati, A. Vital, U. E. Klotz, B. Bommer, T. Graule and M. Winterer, *Powder Technol.*, **165**(2), 73 (2006).
17. W. An, E. Thimsen and P. Biswas, *J. Phys. Chem. Lett.*, **1**(1), 249 (2010).